Journal of Coastal Research	25	1	80–90	West Palm Beach, Florida	January 2009

Calibration of a Lagrangian Transport Model Using Drifting Buoys Deployed during the *Prestige* Oil Spill

Ana J. Abascal, Sonia Castanedo, Fernando J. Mendez, Raul Medina, and Inigo J. Losada

Environmental Hydraulics Institute
(IH Cantabria), Universidad de Cantabria
Avda. de los Castros s/n 39005
Santander, Spain
abascalaj@unican.es

ABSTRACT

ABASCAL, A.J.; CASTANEDO, S.; MENDEZ F.J.; MEDINA, R., and LOSADA, I.J., 2009. Calibration of a Lagrangian transport model using drifting buoys deployed during the *Prestige* oil spill. *Journal of Coastal Research,* 25(1), 80–90. West Palm Beach (Florida), ISSN 0749-0208.

The experience acquired in the *Prestige* crisis management has demonstrated the importance of forecasting oil slick trajectories to plan an effective oil spill response. To have a reliable prediction system, we need to perform a detailed calibration and validation of the oil spill transport model. In this work, the Lagrangian transport model, PICHI, developed by the University of Cantabria during the *Prestige* accident, is calibrated by means of an automatic calibration methodology. The shuffled complex evolution method, developed by the University of Arizona (SCE-UA), is applied to estimate the optimal coefficients of the model. The calibration of the model has been carried out using 13 buoys deployed in the Bay of Biscay during the *Prestige* accident as well as coetaneous meteorological and oceanographic data. Moreover, reanalysis data collected in the Spanish ESEOO project framework has also been used. Results suggest that buoys outside the continental slope were mainly driven by wind, whereas ocean currents played an important role in the motion of the buoys located over the continental slope and shelf. According to these findings, the final calibration of the coefficients is performed considering different buoy data. The methodology applied to this broad buoy database, has allowed us to calibrate the model, taking into account the relative importance of the forcings in buoy movement as well as the dynamics associated with each area.

ADDITIONAL INDEX WORDS: *Wind drag coefficient, wave drag coefficient, Lagrangian transport model, automatic calibration, Prestige accident, buoy trajectories.*

INTRODUCTION

In the last decades the Spanish coast has been affected by many severe oil spills: *Urquiola,* 1976; *Andros Patria,* 1978; *Aegean Sea,* 1992; and most recently, the *Prestige* accident in 2002 (see Figure 1). The *Prestige* oil tanker accident caused one of the largest catastrophes related to oil pollution on the Spanish coast. The *Prestige,* carrying approximately 77,000 t of heavy oil, began to leak approximately 30 nautical miles off the Galician coast (CEDRE, 2002) on November 13, 2002. The ship split in half and sank on November 19, spilling approximately 11,000 t of oil (MONTERO *et al.*, 2003). The latest estimate of the amount of oil spilled until August 2003 was 63,000 t (CASTANEDO *et al.*, 2006) affecting more than 2000 km of shoreline (MINISTERIO DE MEDIO AMBIENTE, 2005).

From the first stages of the accident, different Spanish institutions and public agencies started to work on the monitoring and forecasting of the oil spill. Several operational forecast systems were built in different regions along the northern coast of Spain with a common objective of helping to manage the crisis (CASTANEDO *et al.*, 2006; GONZALEZ *et al.*, 2006; MONTERO *et al.*, 2003). To track the biggest oil slick trajectories and to provide field data to the forecasting systems, the National Spanish Research Council (CSIC) and the Basque Country Technology Institute for Fishing and Food Resources (AZTI) organized the deployment of a set of satellite-tracked Lagrangian floats in December 2002. These buoy data were particularly useful in calibrating the oil spill dispersion models and also for tracking some of the biggest spills (GARCÍA-LADONA *et al.*, 2005).

The experience acquired in the *Prestige* crisis management has demonstrated the importance of forecasting oil slick trajectories when planning an effective oil spill response. To have a reliable prediction system, one has to perform a detailed calibration and validation of the oil spill transport model. Usually, because of the difficulties in obtaining data from real oil spills, the calibration of this kind of model is done using drifter buoys (AL-RABEH, LARDNER, and GUNAY, 2000; COX, 2004; GILBERT, 2004; PRICE *et al.*, 2006).

In this work the calibration of a Lagrangian transport model by means of an automatic calibration methodology is presented. Specifically, the methodology is applied to the Lagrangian transport model, PICHI, developed by the Universidad de Cantabria during the *Prestige* accident as part of its operational forecasting system. Model calibration is performed by means of meteorological and oceanographic numerical data as well as a great number of buoys deployed during the *Prestige* accident. This broad dataset has also allowed the study of the relative importance that the different

DOI: 10.2112/07-0849.1 received 15 March 2007; accepted in revision 2 August 2007.

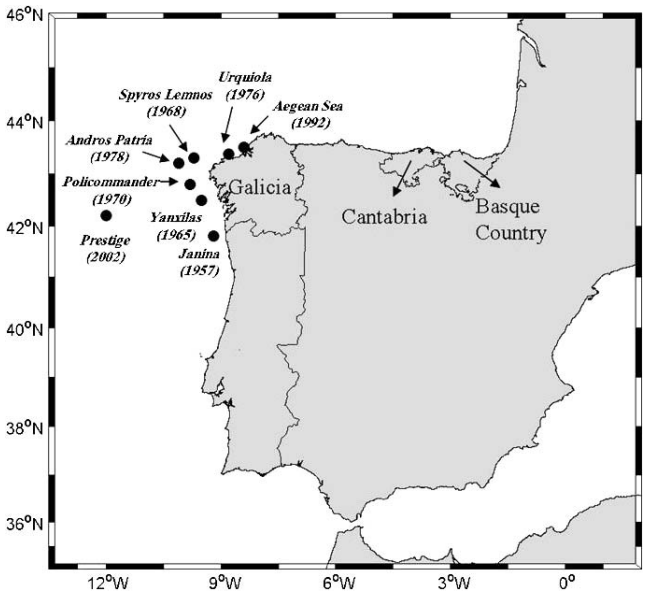

Figure 1. Some of the oil spills have affected the northern and northwestern coast of Spain in the last decades (adapted from CEDRE, 2002). Location of Galicia, Cantabria, and Basque country regions.

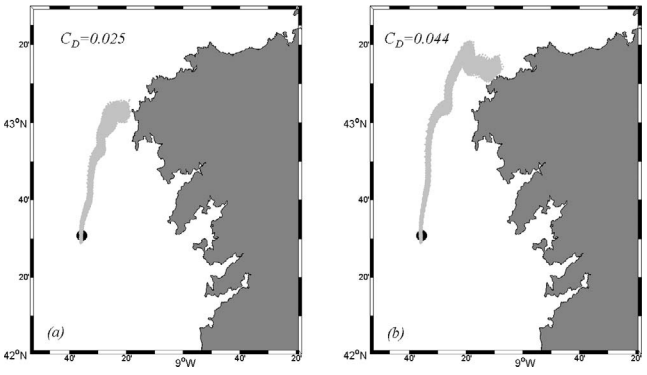

Figure 2. Oil spill simulation with $C_D = 0.025$ (panel *a*) and 0.044 (panel *b*) (black circles indicate the initial position). It can be observed that the stranding point strongly depends on the wind drag coefficient selected.

forcings have on the transportation of drifters. The remainder of this article is organized as follows. Section 2 presents the relevance of the drag coefficients in a Lagrangian transport model, focusing on their importance in the forecast of oil spills. Section 3 presents the data set used in this work. Section 4 presents the description of the oil spill model. Section 5 shows the methodology used for the automatic calibration of the model, including a brief explanation of the optimization method. Section 6 presents the experiments performed. Section 7 summarizes the main conclusions of the study.

RELEVANCE OF DRAG COEFFICIENTS IN A LAGRANGIAN TRANSPORT MODEL

In a Lagrangian model, the oil spill motion is computed by means of the transport induced by surface currents, wind, wave fields, and turbulent diffusion. Usually, this is done using parameters to link the forcing to the oil slick's movement. Accordingly, to simulate the movement of an oil slick, we assume the transport to be composed of an advective and a diffusive velocity. The advective velocity depends on the currents and wind velocity, and the sea state. The diffusive velocity depends on the sea turbulence characteristics. Usually, the latter is simulated as a Brownian motion of particles by means of a random walk procedure (García-Martínez *et al.*, 1999; Koutitas, 1988; Lonin, 1999).

Therefore, assuming a partial transference of momentum from wind and waves, the advective velocity of the oil slick, $\vec{u}_a$, can be expressed as

$$\vec{u}_a = \vec{u}_c + C_D\vec{u}_w + C_H\vec{u}_H, \quad (1)$$

where $\vec{u}_c$ is the surface current velocity, $\vec{u}_w$ is the wind velocity at a height of 10 m over the sea surface, $\vec{u}_H$ is the wave-induced Stokes drift, C_D is the wind drag coefficient, and C_H is the wave coefficient.

In the literature related to this topic, C_D varies from 2.5 to 4.4% of the wind speed, with a mean value of 3–3.5% (ASCE, 1996). Reed, Turner, and Odulo (1994) suggests that in light winds without breaking waves, 3.5% of the wind speed in the direction of the wind gives a good simulation of oil slick drift in offshore areas. Usually wind and wave effects are normally lumped together and represented by the wind drag coefficient. The specific role of waves in the slick's drift has been pointed out by several authors. Sobey and Barker (1997) showed the importance of wave-driven transport in nearshore areas. They consider the wave-driven transport to be a relevant process to be taken into account because it provides a natural mechanism for beaching of surface oil. Castanedo *et al.* (2006) found that although wind drift and surface currents were the major advective transport mechanisms in the Cantabrian Sea, swell wave-induced Stokes drift, noncorrelated with local wind waves, could not be discarded. They found that a C_H around 0.05–1.5% of the wave-induced Stokes drift provided the best fit between the numerical predicted trajectories and the buoys' paths.

Results from models that solve Equation (1) are very sensitive to the value of the drag coefficients. As an example, in Figure 2, two simulations of an oil spill drift, using different wind drag coefficients, are compared. The oil spill was supposed to be 65 km off the Galician coast. The simulated trajectories stand for 3-day predictions. Figures 2a and 2b show the results using wind drag coefficients of 0.025 and 0.044, respectively. It is clear that for the 0.044 wind drag coefficient, the oil slick moves faster. Both simulations predict oil stranding on the northern coast of Galicia. However, the arrival points are separated by about 20 km. It has to be remarked that both wind drag coefficients are in the interval reported by the bibliography (ASCE, 1996; Sobey and Barker, 1997). Any of these values could be used to predict an oil spill trajectory, and as has been shown, different results in time and location of the oil landing can be obtained. This simple experiment makes clear the importance of obtaining the best agreement model coefficients for the region of inter-

Table 1. *Buoys deployed during the* Prestige *accident from December 2002 to January 2003.*

Buoy Number	Buoy Model	Institution	Longitude	Latitude	Initial Date
16751	SC40	LIM(UPC)[1]/ICM(CSIC)[2]	9°25.10′ W	42°52.00′ N	19/12/2002
16752	SC40	LIM(UPC)/ICM(CSIC)	9°25.00′ W	43°05.00′ N	19/12/2002
16753	SC40	LIM(UPC)/ICM(CSIC)	9°34.90′ W	42°57.00′ N	19/12/2002
16754	SC40	LIM(UPC)/ICM(CSIC)	9°35.30′ W	42°40.10′ N	19/12/2002
23282	SC40	ICM(CSIC)	3°20.86′ W	45°15.15′ N	02/01/2003
23289	SC40	ICM(CSIC)	4°00.56′ W	45°34.45′ N	02/01/2003
23348	SC40	ICM(CSIC)	9°25.00′ W	42°51.90′ N	11/01/2003
23258	SC40	ICM(CSIC)	9°34.70′ W	42°39.80′ N	11/01/2003
23249	SC40	ICM(CSIC)	12°03.00′ W	42°12.36′ N	16/01/2003
23259	SC40	ICM(CSIC)	12°03.50′ W	42°10.50′ N	27/01/2003
16651	PTR	AZTI/CEDRE	−3°31.00′ W	44°16.00′ N	27/12/2002
16735	PTR	AZTI/CEDRE	−6°35.00′ W	45°10.00′ N	29/12/2002
16291	PTR	AZTI/CEDRE	−5°52.00′ W	45°18.00′ N	15/01/2003

[1] Maritime Engineering Laboratory of the Technical University of Cataluña.
[2] Marine Research Institute (National Spanish Research Council).

est. Inappropriate values for the model parameters may induce important differences in oil spill forecasting. To achieve a successful oil spill model application and to provide decision-makers with reliable results, we must estimate the optimal coefficients for the area of study.

DATA

Buoys

As mentioned in the previous sections, a set of satellite tracked Lagrangian floats was deployed during the *Prestige* oil spill. The buoys were released between December 2002 and January 2003. Most of them were placed near the Galician coast to track the biggest *Prestige* oil slicks right after the accident, and some of them were used to infer the path of potential spills of the remaining fuel in the wreck. The first group of buoys was deployed on December 19, one month after the sinking of the *Prestige.* A summary of the buoys' data set is presented in Table 1, including drifter number, drifter model, owner institution, and date and position of the first record.

As can be seen in Table 1, six of the buoys were released near the Galician coast, two of them at the tanker sinking point and the rest of them were dropped in the Bay of Biscay. The SC40 surface buoys were implemented with four small pieces of lead to reduce their buoyancy, thereby increasing their efficiency for tracking the spills (García-Ladona *et al.*, 2005). A first set of 4 buoys was deployed on December 19 and a second set of 6 buoys, in groups separated by 10 days. Raw data were collected and preprocessed, and the information was redistributed through a Web server to the regional forecast systems and public agencies.

The last group of buoys, listed in Table 1, was deployed in the framework of an AZTI-CEDRE (French Centre of Documentation, Research and Experimentation on Accidental Water Pollution) cooperation (Girin *et al.*, 2004; Gouriou *et al.*, 2004). This group was composed of four PTR model surface drifters (Girin *et al.*, 2006). Data from these buoys were used to monitor the Bay of Biscay oil slick's evolution. All the buoys were tracked by the ARGOS system onboard the NOAA satellites, and their positions were recorded every hour.

All the buoy trajectories are displayed in Figure 3. Buoys 23249 and 23250, released over the wreck location, moved to the south and drifted away off the Galician coast. The buoys released in the Iberian shelf drifted around Cape Finisterre into the Bay of Biscay following the coastal and shelf shape according to the main trend of the poleward Portugal coastal countercurrent (Haynes and Barton, 1991; Martins, Hamann and Fiúza, 2002). A detailed explanation about the buoys' motion can be found in García-Ladona *et al.* (2005).

Currents

Two current data sets from two global oceanographic models were available in this study, namely, NRLPOM and MERCATOR. NRLPOM (Peggion, Fox, and Barron, 2002) is a version of the Princeton Ocean Model (POM) (Blumberg and Mellor, 1987) that has been implemented at the Naval Research Laboratory (NRL, USA). The model is used to provide relatively high-resolution short-term forecasts, including the effects of tidal forcing (Fox *et al.*, 2001). A specific application for the north of Spain, the NRLPOM-Cantabric model, was developed by the NRL during the *Prestige* accident. The initial conditions of NRLPOM were provided by the global NCOM model (Barron *et al.*, 2006). The boundary conditions were specified from the initial conditions, with the addition of the tidal signal derived from the Grenoble tidal model and updated every time step. The model uses 25 sigma levels, with 19 sigma-coordinate layers in the upper 137 m, and 21 z-level coordinate levels below. The NRLPOM data span December 2002 to December 2003 and correspond to a 48-h forecast of velocity and direction of surface currents. The data consist of instantaneous snapshots with time steps of 3 h in a 0.05° grid resolution. These data were sent daily from the NRL to State Ports of Spain (PdE) during the *Prestige* crisis.

The second set of numerical currents was simulated using the MERCATOR model (Mercator, 2008) corresponding to the version PSY2V1 (Bahurel *et al.*, 2001). The model resolution is 1/12 degree with 43 vertical levels. The data consist of the mean daily velocity and direction of surface currents, and correspond to reanalysis data from November 2002 to March 2003 for the northern coast of Spain. These data have

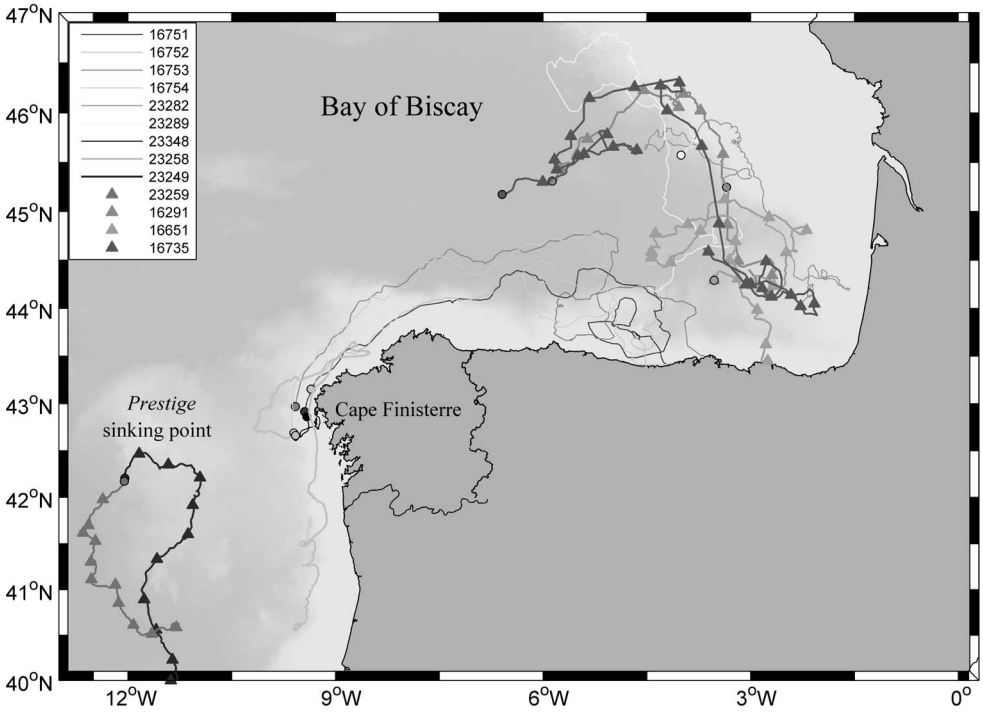

Figure 3. Buoy trajectory evolution during the study period. The drifter identification numbers are indicated on the legend. **For a color version of this figure, see page 149.**

been provided to the authors by PdE in the framework of the Spanish Project, ESEOO (2008).

The opportunity of having data from two state-of-the-art global ocean models allows the study not only of the relative role of each forcing in the trajectories' simulation, but also of the differences attributable to each model used.

Wind and Wave Data

The meteorological data were provided by the Spanish Meteorological Agency (AEMET) in the ESEOO project framework. The data correspond to a wind reanalysis for the November 2002–November 2003 period. The wind fields are the output of the third generation HIRLAM model (CATS and WOLTERS, 1996). The resolution of the model is 0.2°, and the results are the 48-h forecast of wind velocity and direction with a 6-h time interval.

Sea state conditions data are the output of the numerical model WAM, a third generation model that computes spectra of random wind-generated waves (KOMEN *et al.*, 1994; WAMDIG, 1998). The WAM model solves the energy transfer equation for the wave spectrum. The model grid resolution is 0.25°, and the results are the 48-h forecast of significant wave height, mean direction, and mean period for sea and swell components with a 6-h time interval. These data were provided daily by PdE to be used for the Cantabrian operational forecasting system during the *Prestige* crisis. Table 2 shows the main characteristics of each data set described.

THE LAGRANGIAN OIL SPILL TRANSPORT MODEL, PICHI

The frequency of accidental oil spills in marine environments has triggered the development of a large number of mathematical models that simulate the transport and fate of oil slicks. The characteristics of these models range from two-

Table 2. *Summary of buoy and numerical data used in this study.*

Data Set	Initial Date	Final Date	Reanalysis	Model	Institution
BUOYS	December 2002	February 2003			ICM(CSIC) LIM(UPC) AZTI CEDRE
CURRENTS	December 2002	December 2003	NO	NRLPOM	NRL
	November 2002	March 2003	YES	MERCATOR	MERCATOR
WIND	November 2002	November 2003	YES	HIRLAM	AEMET
WAVES	December 2002	December 2003	NO	WAM	PdE

dimensional (2D) particle-tracking models [GNOME (NOAA, 2002), PICHI (Castanedo *et al.*, 2006)] to more complex models that simulate the three-dimensional oil spill trajectory describing the physics of the oil spill processes [OILMAP (ASA, 1997), MOHID (Miranda *et al.*, 2000), MOTHY (Daniel *et al.*, 2003)]. However, when rapid response is required, models like GNOME (NOAA, 2002), a widely used 2D oil spill trajectory model that simulates oil movement due to winds, currents, and tides, may be an excellent choice.

The model used in this work is the two dimensional Lagrangian transport model, PICHI (Castanedo *et al.*, 2006), developed by the Universidad de Cantabria to forecast the *Prestige* oil spill trajectory in the Bay of Biscay. The objective of the model is to simulate the motion of floating objects such as drifters or oil slicks on the water surface. Other aspects like oil weathering or the motion of submerged fuel are not taken into account. In the PICHI model, the drift process of the spilled oil is described by tracking numerical particles equivalent to the oil slicks by means of the transport equation for nonweathering hydrocarbons [Equation(2)].

Each time step, the new position of the particles is computed by the superposition of the transport induced by the mean flow, tides, wind and waves, and turbulent dispersion. The numerical model solves the following vector equation:

$$\frac{d\vec{x}}{dt} = \vec{u}_a(\vec{x}_i, t) + \vec{u}_d(\vec{x}_i, t), \tag{2}$$

where $\vec{x}_i$ is the particle position, and $\vec{u}_a$ and $\vec{u}_d$ are the advective and diffusive velocities, respectively, in $\vec{x}_i$.

The turbulent diffusive velocity is obtained using a Monte Carlo sampling in the range of velocities $[-\vec{u}_d, \vec{u}_d]$ that are assumed proportional to the diffusion coefficients (Hunter, Craig, and Phillips, 1993; Maier-Reimer, 1982). The velocity fluctuation for each time step is defined in the following way:

$$|\vec{u}_d| = \sqrt{\frac{6D}{\Delta t}}, \tag{3}$$

where D is the diffusion coefficient.

The advective velocity is calculated as the linear combination of currents and wind velocity and swell wave drift, expressed as

$$\vec{u}_a = C_C\vec{u}_c + C_D\vec{u}_w + C_H\vec{u}_H. \tag{4}$$

Note that Equation (4) is not the same as Equation (1). The latter includes a coefficient in the currents term C_C that does not appear in Equation (1). Usually in Lagrangian models the current term is not affected by any coefficient. However, because the current data available for this work come from numerical model results (NRLPOM and MERCATOR) and to take into account that results from both models were not coincident and that there is an inherent uncertainty in the outputs of any model, it was decided to include a calibration coefficient for the current velocity to minimize the differences between actual and numerical trajectories.

Another difference between Equations (4) and (1) is that the wave transport in Equation (4) stands only for the swell wave-induced Stokes drift. Therefore, the wind drag coefficient C_D stands for a wind induced drift C_{Dw}, and it also includes a surface drift induced by sea waves generated by local winds, C_{DH}. Typically, the wind drag coefficient is assumed to be $C_{Dw} = 0.03$. Moreover, Sobey and Barker (1997), established that the surface wave drift can be estimated by $0.015u_w$ ($C_{DH} = 0.015$). Therefore, considering both effects, $C_D = C_{Dw} + C_{DH}$, the typical wind drag coefficient value of 0.03 may increase to 0.04 or 0.05 to combine wind and wave drift. However, this approach remains appropriate only while the waves are directly related and propagate in the same direction as the local wind. This is not the case for swell waves, and therefore in the PICHI model the transport induced by swell waves is calculated following Dean and Dalrymple (1991) as

$$u_H = \frac{2\pi H}{8T}, \tag{5}$$

where H is the significant wave height and T is the mean period. Considering a partial transference of the swell wave current to the effective drift, a coefficient wave C_H was included and calibrated.

Substituting Equation (4) in Equation (2) and expressing the system by means of the Euler method, the position of the particles at every time step is expressed as

$$\vec{x}_i^{n+1} \cong \vec{x}_i^n + \Delta t[C_C\vec{u}_c(\vec{x}_i^n, t^n) + C_D\vec{u}_w(\vec{x}_i^n, t^n) + C_H\vec{u}_H(\vec{x}_i^n, t^n) + \vec{u}_d(\vec{x}_i^n, t^n)], \tag{6}$$

where C_C, C_D, and C_H are the model parameters to be calculated in the calibration process.

AUTOMATIC CALIBRATION METHODOLOGY

The model calibration can be performed by means of a trial-and-error procedure. In this process the simulated trajectories are fitted to the real buoys' paths to adjust the model parameters. Because of the large number of buoys deployed and the great amount of variables involved in the analysis, this procedure becomes a laborious and intensive job. To avoid this problem, in this work we used an automatic calibration to find the best model coefficients. To do this, we applied a global optimization methodology.

The shuffled complex evolution method (Duan, Sorooshian and Gupta, 1992) developed by the University of Arizona (SCE-UA) has been applied to estimate the optimal coefficients of the oil spill model. This method has been used in an effective way in the resolution of highly nonlinear problems and is widely used in the automatic calibration of watershed models. The SCE-UA method is based on a synthesis of four concepts: (1) a combination of deterministic and probabilistic approaches; (2) a systematic evolution of a "complex" of points spanning the parameter space in the direction of global improvement, (3) competitive evolution; (4) complex shuffling. The synthesis of these elements makes the SCE-UA method effective and robust, and also flexible and efficient.

Following this methodology, the oil spill model calibration was formulated as an optimization problem where an objective function J has to be minimized. In this case, the objective function was defined as

$$J(\theta) = \sum_{j=1}^{T}\sum_{i=1}^{N}\{[U_{Bx}(\vec{x}, t) - U_{Mx}(\vec{x}, T, \theta)]^2 + [U_{By}(\vec{x}, t) - U_{My}(\vec{x}, t, \theta)]^2\}. \tag{7}$$

Table 3. *Buoy number and record length used for the calibration experiments. These sections were selected as a function of the wind, current, and wave data availability.*

Buoy Number	Initial Date	Final Date	Record Length (h)
16751	19/12/2002	31/01/2003	233
16752	19/12/2002	19/01/2003	141
16753	19/12/2002	30/01/2003	230
16754	19/12/2002	01/02/2003	233
23282	02/01/2003	18/02/2003	296
23289	02/01/2003	18/02/2003	157
23348	11/01/2003	25/01/2003	32
23258	11/01/2003	19/02/2003	162
23249	16/01/2003	19/02/2003	86
23259	27/01/2003	19/02/2003	39
16291	15/01/2003	09/02/2003	101
16651	27/12/2002	03/02/2003	202
16735	29/12/2002	19/02/2003	261

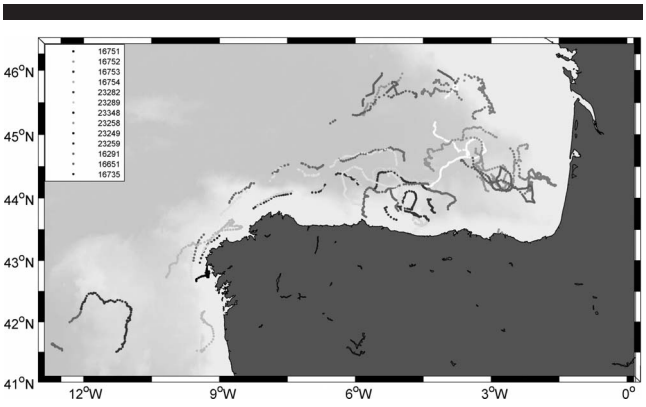

Figure 4. Trajectory sections selected for the analysis (December 2002–February 2003). **For a color version of this figure, see page 149.**

Equation (7) represents the difference between the predicted trajectories and the buoy paths. U_{BX} and U_{BY} are the buoy velocity components in the x (W-E) and y (N-S) direction, respectively; U_{Mx} and U_{My} are the model velocity components in the x and y direction, respectively; T is the period with buoy data; N is the number of analyzed buoys, and $\theta = (C_H, C_D, C_C)$ is the vector of parameters to be obtained.

The buoy velocity $\vec{U}_B$ was obtained from the satellite tracked positions

$$\vec{U}_B = \frac{\sum_{t=i}^{i+2} (x_{t+dt} - x_t)}{\Delta t}, \tag{8}$$

where $\vec{x}$ is the buoy position at the time t, dt is 1 h corresponding to the temporal resolution of the buoy data, and Δt corresponds to a 3-h time step.

The advective model velocity $\vec{U}_M$ was estimated by means of the numerical data provided by the models. Wind, current, and wave data were interpolated to each buoy position, using:

$$U_{Mx} = C_C u_{cx} + C_D u_{wx} + C_H u_{Hx}, \tag{9}$$

$$U_{My} = C_C u_{cy} + C_D u_{wy} + C_H u_{Hy}, \tag{10}$$

C_C and C_H were assumed to be constant coefficients. Usually, C_D is considered as a constant coefficient (Sobey and Barker, 1997). However, in this work a variable wind drag coefficient is proposed. An estimation of C_D as a linear function of the wind speed was considered,

$$C_D = \alpha + \beta|\vec{u}_w|. \tag{11}$$

Equation (11) introduces two new parameters, α and β, to be included in the calibration analysis. Previous tests (not shown here) using a coefficient for the diffusive velocity were performed, but the results were practically the same.

Substituting Equations (9), (10), and (11) in Equation (7) leads to

$$J(\theta) = \sum_{j=1}^{T} \sum_{i=1}^{N} \left[\{U_{Bx} - [C_H U_{Hx} + (\alpha + \beta|\vec{U}_w|)U_{wx} + C_C U_{cx}]\}^2 + \{U_{By} - [C_H U_{Hy} + (\alpha + \beta|\vec{U}_w|)U_{wy} + C_C U_{cy}]\}^2 \right]. \tag{12}$$

The aim of the automatic calibration was to find the optimal combination of the vector parameter $\theta = (C_H, \alpha, \beta, C_C)$ that minimizes the objective function J.

RESULTS

As a first step, a revision of the database was performed. As was shown in Table 1, buoy data span December 2002 to February 2003, but because numerical wind, waves, and current data have some gaps, a selection of appropriate experiment dates was required. Table 3 shows the dates with available buoy and numerical data. Figure 4 displays the buoy trajectories for the chosen dates.

Wind, waves, and current data were spatially interpolated to the buoys' positions (Figure 4). In summary, the database for the experiments included 2173 buoy positions (each trajectory has many positions), and wind, current, and wave velocities (interpolated to each buoy position) with a 3-h temporal resolution (minimal resolution of numerical data corresponding to the NRLPOM currents).

Once this data processing was done, buoy, wind, current, and wave velocities were introduced into Equation (12) to calculate the calibration coefficients of the model.

Results Considering All Buoys

To have a preliminary vision of the relationship between numerical and measured data, we calculated the optimal combination of coefficients considering all the buoys and the NRLPOM data. The coefficients minimizing the objective function were found to be $C_H = 0.068$, $\alpha = 0.022$, $\beta = 0.0000644$, and $C_C = 0.266$. Note that although a linear variation of C_D as a function of the wind speed was proposed [Equation (11)], the small value obtained for the β coefficient suggests that, in this case, C_D was a constant factor represented by α. Furthermore, it is important to remark that the obtained value for C_D is smaller than typical values reported in the bibliography (Sobey and Barker, 1997). Also note the small value of C_C. Several explanations can be proposed for this small value. The first one is that the surface current and the wind are codirectional and the optimization scheme gives all the weight to the wind term. The second possibility is that

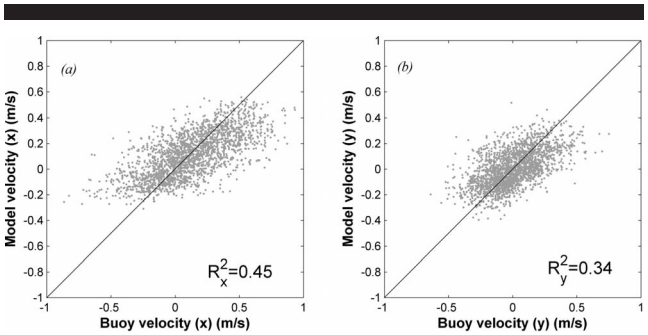

Figure 5. Correlation factors between buoy and numerical velocity. (a) R_x^2, correlation factor for the velocity component in the x direction (W-E) and (b) R_y^2, correlation factor for the velocity component in the y direction (N-S).

the current results provided by the oceanographic model presents such a deviation from data that the optimization scheme tries to avoid using that current value.

The relative importance of the wind surface drag, surface currents, and swell wave-induced Stokes drift in the advective model velocity was estimated as $C_D \mid \vec{u}_W \mid / \mid \vec{U}_M \mid$, $C_C \mid \vec{u}_C \mid / \mid \vec{U}_M \mid$, and $C_H \mid \vec{u}_H \mid / \mid \vec{U}_M \mid$, using the C_H, C_C, and C_D values previously obtained. The analysis shows that 79% of the advective velocity is due to the wind surface velocity, 9% to the surface current, and 12% to the swell wave-induced Stokes drift. This result makes clear the dominance of the surface wind velocity over waves and current forcing. However, it is also remarked that 12% of the advective model velocity is due to the Stokes drift, meaning that the wave forcing could not be discarded in the buoy trajectories' simulations.

The correlation factor between the model and buoy velocity components was calculated. Scatter plot and the associated correlation factors for u (R_x^2) and v (R_y^2) components are presented in Figure 5. It is observed that the correlation is less than 0.5 for both components. To make a vectorial comparison between the model and the buoy velocity, we calculated the vector correlation factor, R^2 (Breaker and Gemmill, 2003). For a two-dimensional case, R^2 varies between 0.0 (no correlation) and 2.0 (perfect correlation). In this case, the vectorial correlation R^2 also showed a low value of 0.83. Therefore, a clear relationship was not found.

Similar analysis was performed using the MERCATOR database (not shown here). The correlation factors between buoys and model velocity using the MERCATOR database was comparable to the correlations obtained with the NRLPOM database (Abascal *et al.*, 2005). Because the temporal resolution of the NRLPOM database (3-h snapshots) is higher than the temporal resolution of the MERCATOR database (daily average), the rest of the experiments were performed with the NRLPOM currents.

The weak correlation obtained in the all buoy experiments indicates the discrepancies between numerical data and real trajectories. The differences between the model and the observations can be due mainly to errors in the numerical input fields (winds, waves, and currents) and to possible location errors of the drifters (Edwards, Werner and Blanton, 2006; Price *et al.*, 2006; Sebastiao and Soares, 2006).

To improve the correlation factors, we carried out the automatic calibration for each buoy.

Single Buoy Results

Next, the application of the automatic calibration method to each buoy is described. These experiments focused on finding patterns and groups of buoys to reduce the large number of variables involved in the problem. Equation (12) was solved to obtain the best fit coefficients in each case. The coefficients and correlation factors (R_x^2, R_y^2, and R^2) calculated in the calibration process are presented in Table 4.

The first point to be emphasized is that the correlation factors are highly variable, ranging from $R^2 = 0.30$ for buoy 23348 to $R^2 = 1.28$ for buoy 16291. Based on these results, buoy data classification was performed as a function of the scalar and vectorial correlation factors. Buoys with $R^2 < 0.9$ were included in Group I and buoys with $R^2 \geq 0.9$ in Group II. Table 4 and Figure 6 show the buoys included in each group. As can be seen in Figure 6, most of the buoys belonging to Group II were deployed off the continental slope. The seasonal mean flow in this area is characterized by surface currents in agreement with the seasonal mean wind-driven Ekman drift (van Aken, 2002). Most of Group I buoys moved over the continental slope or shelf. This area is characterized by a stronger, poleward slope current in winter (van Aken,

Table 4. *Calibration coefficients (C_H, $C_D = \alpha + \beta|\vec{u}_w|$, and C_C), and correlation factors obtained for each buoy.*

Group	Buoy Number	C_H	α	β	C_C	R^2_x	R^2_y	R^2	R^2_{WC}
I	16751	0.157	0.019	−0.000385	0.455	0.14	0.19	0.49	0.36
	16752	0.443	0.020	0.0000211	0.573	0.33	0.24	0.64	0.32
	16753	0.270	0.0075	0.001	0.245	0.33	0.41	0.86	0.27
	16754	0.087	0.026	−0.00041	0.410	0.39	0.34	0.78	0.26
	23282	0.048	0.017	0.000586	0.079	0.53	0.26	0.81	0.72
	23289	−0.0375	0.029	0.00053	−0.154	0.42	0.27	0.72	0.24
	23348	0.048	−0.009	0.003	0.44	0.004	0.23	0.30	0.63
	23258	0.036	0.025	−0.000218	0.427	0.52	0.46	0.85	0.70
	23249	0.017	0.029	−0.000818	0.51	0.52	0.43	0.87	0.80
II	23259	−0.196	0.028	−0.00076	0.084	0.75	0.34	0.90	0.71
	16291	0.100	0.021	0.00046	0.316	0.60	0.62	1.28	0.33
	16651	−0.124	0.021	0.00069	−0.009	0.64	0.51	1.19	0.41
	16735	−0.019	0.016	0.00115	0.113	0.59	0.41	1.05	0.27

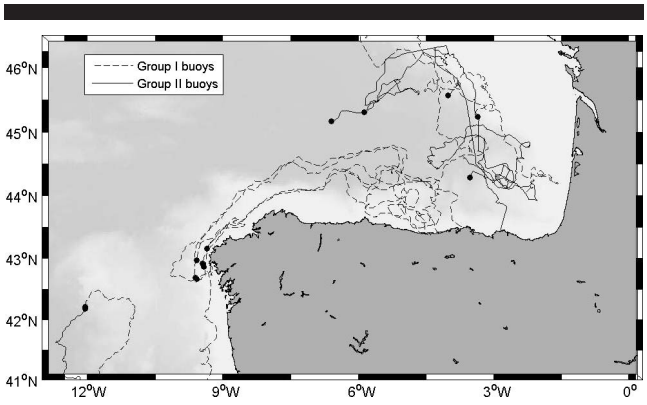

Figure 6. Group I buoys (dashed lines) and Group II buoys (solid lines) are presented. Initial positions are represented by black circles. Group I buoys were mainly deployed over the continental slope, whereas Group II buoys were outside of the continental slope.

2002), which forms an extension of the seasonal slope current along the ocean margins of Portugal and Spain (FROUIN *et al.*, 1990).

Also noteworthy is the wide range of values obtained for the currents coefficient, C_C (see Table 4). This coefficient ranges from negative values (buoy 23289, 16651) to a maximum of 0.57 (buoy 16752). As mentioned previously, small C_C values may be explained by codirectional wind and surface currents or by the low relation between the current data and the buoy trajectories. To find which of these two explanations is the correct, we estimated the vectorial correlation coefficient between wind and surface current velocities (R^2_{WC}) (see Table 4). The lower R^2_{WC} values obtained (smaller than 1) suggest a weak relation between the wind and current velocity directions.

In general, Group II have small current coefficients and high correlation factors R^2. These small C_C values suggest that the weak currents existing off the continental slope play a negligible role in buoy trajectory simulations. In spite of this, the high correlation factors in this group indicate a good agreement between actual and predicted trajectories, suggesting that numerical wind data are well correlated with buoy trajectories.

On the contrary, Group I presents the higher current coefficients and the lower correlation factors, meaning that to reproduce these buoy trajectories, we have to consider a joint wind and current effect. The highest current coefficient, C_C, corresponds to buoy 16752. This buoy and the 16751, 16753, and 16754 buoys were deployed in front of the Finisterre cap over the continental slope region (Figure 3). After the deployment, these buoys contoured the corner of the Iberian Peninsula and entered the Biscay Bay following the coastal and shelf geometry. This pattern is coherent with the dynamics of the southern region of the Bay of Biscay that presents the most intense surface fluxes from October to February (PINGREE AND LE CANN, 1990). Advanced, very high resolution radiometer images taken in November 2002 and January 2003 show that the poleward current warm water (DESCHAMPS, FROUIN AND CRÉPON, 1984; PINGREE and LE CANN, 1990) entered the Bay of Biscay around Galicia and extended eastward along the Cantabrian shelf and slopes (GARCÍA-SOTO, 2004). Considering the region dynamics, it is not surprising to find the highest current influence for the buoys located over the continental slope. Also, the complex pattern that characterized the slope currents along the Cantabrian shelf combined with the coarse grid resolution used in the current numerical models could explain the low correlation factors obtained in Group I.

Table 5. *Outer buoys number and records length used to calculate C_H and C_D.*

Buoy Number	Record Length (h)
23259	39
16291	44
16651	96
16735	117

The mean relative importance of the forcings in the advective model was estimated for each group using the C_H, C_C, and C_D values shown in Table 4. For Group I, 64% of the advective model velocity is due to the wind surface velocity, 21% to the surface current, and 15% to the swell wave-induced Stokes drift. However, in Group II, 80% of the advective model velocity is explained by the wind surface velocity; meanwhile the surface current and the swell wave-induced Stokes drift represents 6 and 13%, respectively. These results along with the high correlation found in Group II (Table 4) suggest that these buoys could be simulated only with the wind.

Best Calibration Coefficients

The objective of this section is to improve the correlation factors previously calculated considering all buoys (see Figure 5). To do this, the conclusions obtained in the two previous sections have been taken into account. First, trajectories located out of the continental slope (hereafter outer buoys) were selected. Based on the previous results suggesting the dominance of the wind forcing in this area (Group II), negligible current effect was assumed. These trajectories, forced mainly by the wind, were used to estimate C_H and C_D by means of the automatic calibration methodology. Table 5 and Figure 7 show the selected buoys and trajectories section lengths (in hours) used in this analysis.

Therefore, assuming that current effects can be neglected with respect to the wind forcing, the objective function J was defined as

$$J(\theta) = \sum_{j=1}^{T} \sum_{i=1}^{N} \left[\{U_{Bx} - [C_H U_{Hx} + (\alpha + \beta|U_w|)U_{wx}]\}^2 + \{U_{By} - [C_H U_{Hy} + (\alpha + \beta|U_w|)U_{wy}]\}^2 \right], \quad (13)$$

where $\theta = (C_H, \alpha, \beta)$ and the summation is extended to the outer buoys. As in the previous analysis, a linear variation for the wind coefficient as well as sea and swell independence was assumed.

The optimal combination of coefficients obtained was $C_H = 0.022$, $\alpha = 0.017$, and $\beta = 0.001$. Note that the swell wave coefficient, C_H, was of the same order of magnitude as that obtained in the experiment performed with all buoys. The C_H

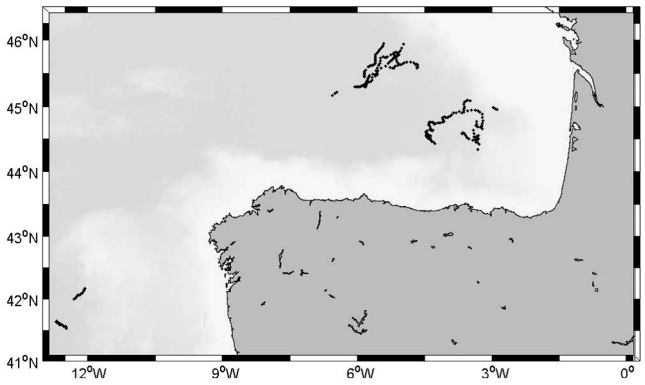

Figure 7. Selected trajectory sections, located out of the continental slope.

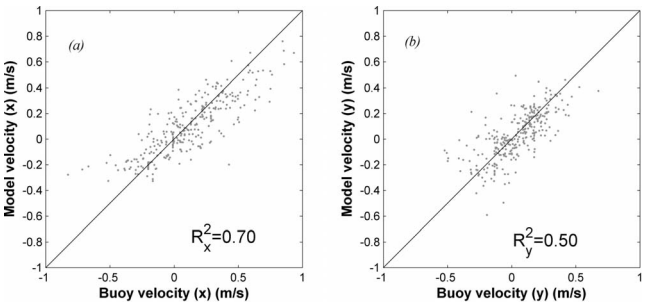

Figure 9. Scatter plots for u (panel a) and v (panel b) components of the buoy and model velocity, with associated correlation factors. Current velocities have been neglected in the analysis.

value obtained was consistent with SOBEY and BARKER (1997). They found that the predicted surface drift for a steady progressive and nonlinear wave train differs by an order of magnitude from the Stokes drift for monochromatic waves [Equation (5)], suggesting that linear theory for regular waves may not provide an adequate estimate of the surface drift. The presented analysis also shows that β is two orders of magnitude bigger than that calculated in the all buoys experiment. Figure 8a shows that, in accord with the initial hypothesis, the wind drag coefficient C_D increases with the wind speed. In Figure 8b, the C_D time variation for each buoy trajectory is plotted. C_D values range from 0.018 to 0.004, with a mean value of 0.027 and a standard deviation of 0.038. These limits are included in the range cited in the bibliography (ASCE, 1996; SOBEY and BARKER, 1997) and are also in accord with previous calibration results of the *Prestige* period (CARRACEDO *et al.*, 2006; CASTANEDO *et al.*, 2006). The need to use a set of different wind drag coefficients to adjust the buoys' trajectories and model predictions has been shown in previous works. For example, during the "Ground Truth" exercise, it was found that the wind factor had to be increased from 0.005 to 0.02 to compensate for higher winds when low current streams were present (GILBERT, 2004).

Figure 9 shows a scatter plot for u and v components obtained in this experiment (outer buoys). Comparing these results with those obtained in the experiment performed with all buoys (Figure 5), we detect an increase of the correlation factors. The correlation factor changes from 0.45 to 0.70 in the x direction and from 0.34 to 0.5 in the y direction. This produces an improvement of the vectorial correlation factor R^2 whose value changes from 0.83 to 1.23. These results suggest a better agreement between numerical data and buoy trajectories located off the continental slope.

CONCLUSIONS

In this paper, a Lagrangian transport model has been calibrated by means of an automatic calibration methodology

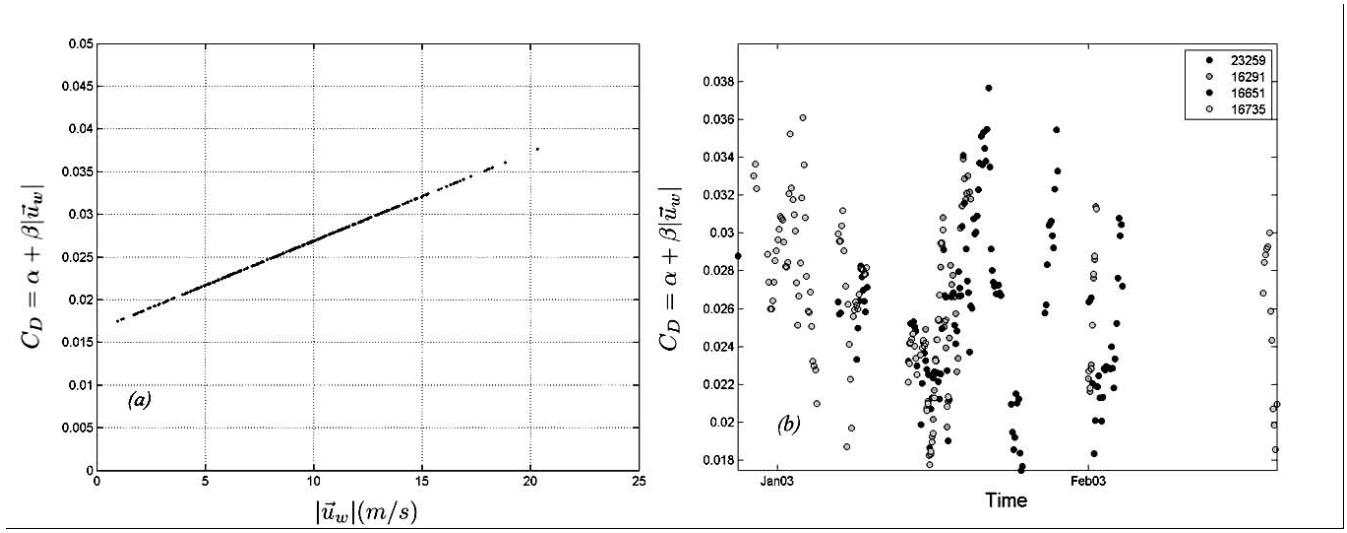

Figure 8. (a) C_D variation as a function of the wind speed; (b) C_D variation for each buoy trajectory.

based on a global optimization algorithm. The wind drag coefficient has been assumed as a linear dependence of the wind speed. To include the wave effect, we separated the wind drag coefficient into sea and swell, considering only the effect of the swell on transport. Normally, the transport models do not include a wave coefficient; however, SOBEY and BARKER (1997) prove that the linear theory overestimates the effect of the wave with regard to the wave spectrum. Taking these results into account, we used a drag coefficient to adjust the swell wave-induced Stokes drift.

Typically, the oil spill models are calibrated using the drag coefficient values reported in the bibliography, or by means of a trial-and-error procedure using a single Lagrangian buoy. The methodology applied here introduces two new concepts. First, no hypotheses regarding the influence of the oil spill processes are assumed. This means that the dominant effect of the wind over the currents and waves is not adopted *a priori* but is the same technique that determines the relative importance of each forcing in the movement. Second, the calibration methodology is based on a spatial approach integrating the information of a large data set of buoys. In this manner, the calibration model utilizes data from buoys located in the study area and the obtained calibration coefficients are representative of the model's area of influence.

Given the uncertainty associated with this kind of problem, in which numerical data from different numerical models are used, the calibration has been performed by means of different tests. Therefore, preliminary experiments were performed considering all buoys and a single buoy calibration. The reliability of the calibration experiments is evaluated by means of the correlation factors.

The experiment performed with all buoys showed weak correlation coefficients (lower than 0.5) between the model and buoy velocity components. Small values of the current coefficient, C_C, were obtained in this experiment. Although two state-of-the-art current databases have been used, the complex pattern that characterized the slope currents, combined with the coarse grid resolution, may explain the discrepancies between the real and numerical current fields, and consequently the low C_C values obtained. The wind and wave drag coefficients obtained in this experiment were discarded because of the low correlation factors.

The single buoy experiments were carried out to find general patterns and groups of buoys to be calibrated together. This analysis revealed that the agreement between the model and buoy velocities was not the same for all buoys. The features of each experiment led us to separate the buoys into two groups (I and II) as a function of the correlation factors. Most of the buoys in Group II ($R^2 \geq 0.9$) were deployed off the continental slope. On the contrary, most of the buoys in Group I ($R^2 < 0.9$) were deployed over the continental slope or shelf. The overall results, supported by the previous knowledge of the area, suggested that buoy trajectories located outward of the continental slope were dominated by the wind forces, whereas ocean currents were an important factor in the motion of the buoys located over the continental slope or shelf.

Finally, the calibration methodology was applied to the buoy trajectories located outside the continental slope to obtain the optimal C_H and C_D. Negligible currents were assumed in this area. The optimal waves and wind coefficients obtained with outer buoys were $C_H = 0.022$ and $C_D = 0.017 + 0.001|\vec{u}_w|$. According to the initial hypothesis, a linear variation of C_D as a function of the wind speed was found. The C_D variation was in the range of 0.018 to 0.038, consistent with the wind drag coefficient values reported in ASCE (1996) and SOBEY and BARKER (1997). The C_H coefficient shows that the swell wave-induced Stokes drift for a monochromatic wave is overestimated by two orders of magnitude. The correlation factors ($R_x^2 = 0.70$ and $R_y^2 = 0.50$) showed that buoy velocities correlated fairly well with numerical velocities; therefore, C_H and C_D were assumed to be the optimal model coefficients for wind and waves.

The single buoy calibration has demonstrated that the optimal coefficients are not constant, changing according to the data used for the adjustment. These differences have shown that the calibration of a model using data from only one data set depends on the space and period of the trajectory of the buoy. In this manner, the utilization of a series of buoys with an ample coverage of the study area has allowed us to obtain calibrated coefficients that are much more representative of the area of application of the model.

ACKNOWLEDGMENTS

This work has partly been funded by the Spanish Ministry of Education and Science under research projects VEM2003-C14-03 (ESEOO project) and TRA2007-65133/TMAR (PREVER project), and by the Marcelino Botin Foundation. S.C. would like to thank the Spanish Ministry of Science and Technology for the support under Ramon y Cajal Program.

LITERATURE CITED

ABASCAL, A.J.; CASTANEDO, S.; MEDINA, R., and LOSADA, I.J., 2005. Calibración de un modelo de transporte Lagrangiano mediante el reanálisis de los datos del *Prestige.* Report of the ESEOO project (in Spanish), www.eseoo.org (accessed October 22, 2008).

AL-RABEH, A.H.; LARDNER, R.W., and GUNAY, N., 2000. Gulfspill Version 2.0: a software package for oil spills in the Arabian Gulf. *Environmental Modelling & Software,* 15, 425–442.

ASA (APPLIED SCIENCE ASSOCIATES), 1997. *OILMAP for Windows* (technical manual). Narrangansett, Rhode Island: ASA Inc.

ASCE (AMERICAN SOCIETY OF CIVIL ENGINEERS), 1996. State-of-the-art review of modeling transport and fate of oil spills, ASCE Committee on Modeling Oil Spills. Water Resources Engineering Division. *Journal of Hydraulic Engineering,* 122(11), 594–609.

BAHUREL, P.; DE MEY, P.; DE PRADA, T.; DOMBROWSKY, E.; JOSSE, P.; LE PROVOST, C.; LE TRAON, P.-Y. ; PIACENTINI, A., and SIEFRIDT, L., 2001. MERCATOR, forecasting global ocean, *AVISO Altimetry Newsletter,* 8, Toulouse, France: CNES, pp. 14–16.

BARRON, C.N.; MARTIN, P.J.; KARA, A.B.; RHODES, R.C., and SMEDSTAD, L.F., 2006. Formulation, implementation and examination of vertical coordinate choices in the Global Navy Coastal Ocean Model (NCOM). *Ocean Modelling,* 11, 437–375.

BLUMBERG, A.F. and MELLOR, G.L., 1987. A description of a three-dimensional coastal ocean circulation model. *In:* HEAPS, N.S. (ed.), *Three-Dimensional Coastal Ocean Models.* Washington, D.C.: American Geophysical Union.

BREAKER, L.C. and GEMMILL W.H., 2003. A curious relationship between the winds and currents at the western entrance of the Santa Barbara Channel. *Journal of Geophysical Research,* 108(C5), 3132.

CARRACEDO, P.; TORRES-LÓPEZ, S.; BARRERIRO, M.; MONTERO, P.; BALSEIRO, C.F.; PENABAD, E.; LEITAO, P.C., and PÉREZ-MUÑUZURI, V., 2006. Improvement of pollutant drift forecast system applied to the *Prestige* oil spills in Galicia coast (NV of Spain): development of an operational system. *Marine Pollution Bulletin,* 53, 350–360.

Castanedo, S.; Medina, R.; Losada, I.J.; Vidal, C.; Méndez, F.J.; Osorio, A.; Juanes, J.A., and Puente, A., 2006. The *Prestige* oil spill in Cantabria (Bay of Biscay). Part I: Operational forecasting system for quick response, risk assessment and protection of natural resources. *Journal of Coastal Research,* 22(6), 1474–1489.

Cats, G. and Wolters, L., 1996. The Hirlam Project. *IEEE Computational Science and Engineering,* 3(4), 4–7.

CEDRE, 2002. Naufrage du Petrolier Prestige, Le lettre du CEDRE, No. 90, http://www.le-cedre.fr/images/02nov.pdf (accessed March 10, 2006).

Cox, 2004. The Prince William Sound 2004 Lagrangian Field Experiment. http://ak.aoos.org/pws/reports/contents.pdf (accessed October 22, 2008).

Daniel, P.; Marty, F.; Josse, P.; Skandrani, C., and Benshila, R., 2003. Improvement of drift calculation in Mothy operational oil spill prediction system. *Proceedings of the 2003 International Oil Spill Conference.* Washington, D.C.: American Petroleum Institute.

Dean, R.G. and Dalrymple, R.A., 1991. *Water Wave Mechanics for Engineers and Scientists.* Advanced Series on Ocean Engineering, vol. 2. Singapore: World Scientific.

Deschamps, P.Y.; Frouin, R., and Crépon, M., 1984. Sea surface temperatures of the coastal zones of France observed by the HCMM satellite. *Journal of Geophysical Research,* 89(C5), 8123–8149.

Duan, Q.; Sorooshian, S., and Gupta, V. 1992. Effective and efficient global optimization for conceptual rainfall-runoff models. *Water Resources Research,* 28(4), 1015–1031.

Edwards, K.P.; Werner, F.E., and Blanton, B.O., 2006. Comparison of observed and modeled drifter trajectories in coastal regions: an improvement through adjustments for observed drifter slip and errors in wind fields. *Journal of Atmospheric and Oceanic Technology,* 23(11), 1614–1620.

ESEOO. Title. http://www.eseoo.org (accessed October 22, 2008).

Fox, D.N.; Barron, C.N.; Carnes, M.R.; Booda, M.; Peggion, G., and Gurley, J.V., 2001. The modular ocean data assimilation system. *Oceanography,* 15(1), 22–28.

Frouin, R.; Fiúza, A.F.C.; Ambar, I., and Boyd, T.J., 1990. Observations of a poleward surface current off the coasts of Portugal and Spain during winter. *Journal of Geophysical Research,* 95(C1), 679–691.

García-Ladona, E.; Font, J.; del Río, E.; Julià, A.; Salat, J.; Chic, O.; Orfila, A.; Alvarez, A.; Basterretxea, G.G.; Vizoso, G.; Piro, O.; Tintoré, J.; Gil, M.; Herrera, J.L., and Castanedo, S., 2005. The use of surface drifting floats in the monitoring of oil spills. The Prestige case. *Proceedings of the 19 Biennial International Oil Spill Conference* (IOSC), Miami, CD-ROM: 14718A.

García-Martínez, R. and Flores-Tovar, H., 1999. Computer modeling of oil spill trajectories with a high accuracy method. *Spill Science & Technology Bulletin,* 5(5–6), 323–330.

García-Soto, C., 2004. '*Prestige*' oil spill and Navidad flow. *Journal of the Marine Biological Association of the United Kingdom,* 84, 297–300.

Gilbert, 2004. Outcomes of the OSTM Ground Truth Exercise and Future Directions. Australian Maritime Safety Authority, 13th National Plan, Environment and Scientific Coordinators Workshop. http://www.amsa.gov.au/Marine_Environment_Protection/National_plan/Environment_and_Scientific_Coordinators_Toolbox/Workshop_Proceedings/2004/Day2/.pdf (accessed January 10, 2007).

Girin, M.; Cabioc'h, F.; Peigne, G.; Gouriou, V.; Abascal, A.J.; Castanedo, S., and Parthiot, F., 2006. Synthese sur la contribution des produits et services satellitaires a la prevision de derive de nappes d'hydrocarbures pour la lutte en mer et a l'information de la terre. Sécrétariat Général pour les Affaires Régionales. INTERREG III B-POST PRESTIGE.

Girin, M.; Cabioc'h, F.; Peigné, G.; Uribe, J.; Menéndez, J.; Pozo, R.; González, M.; Uriarte, A., and Castanedo, S., 2004. Exchanging Information for Improved Response and Public Communication in a Transboundary Oil Spill: The Prestige Experience. *Interspill 2004,* p, 403, Trondheim, Norway.

González, M.; Uriarte, A.; Pozo, R., and Collins, M., 2006. The *Prestige* crisis: operational oceanography applied to oil recovery, by the Basque fishing fleet. *Marine Pollution Bulletin,* 53, 369–374.

Gouriou, V.; Cabon, R.; Gieu, V.; Girardot, A.L., and Lepetit, A., 2004. Data management system concerning both pollution monitoring and response operations during an oil spill: the *Prestige* experience. *Interspill 2004,* p. 405, Trondheim, Norway.

Haynes, R. and Barton E.D., 1991. Lagrangian observations in the Iberian coastal transition zone. *Journal of Geophysical Research,* 96(C8), 14731–14741.

Hunter, J.R.; Craig, P.D., and Phillips, H.E., 1993. On the use of random walk models with spatially variable diffusivity. *Journal of Computational Physics,* 106, 366–376.

Komen, G.J.; Cavaleri, L.; Donelan, M.; Hasselmann, K., and Janssen, P.A.E.M., 1994. *Dynamics and Modeling of Ocean Waves.* Cambridge, UK: Cambridge University Press.

Koutitas, C.G., 1988. *Mathematical Models in Coastal Engineering.* Pentech Press, London.

Lonin, S.A., 1999. Lagrangian model for oil spill diffusion at sea. *Spill Science & Technology,* 5, 5–6, 331–336.

Maier-Reimer, E., 1982. On tracer methods in computational hydrodynamics. *In:* Abbott, M.B. and Cunge, J.A. (eds.), *Engineering Application of Computational Hydraulics,* vol. 1, chap 9. London: Pitman.

Martins, C.S.; Hamann, M., and Fiúza, A.F.G., 2002. Surface circulation in the eastern North Atlantic, from drifters and altimetry. *Journal of Geophysical Research,* 107(C12) 3217, doi: 10.1029/2000JC000345.

Mercator. Title. http://www.mercator-ocean.fr (accessed October 22, 2008).

Ministerio de Medio Ambiente, Dirección General de Costas, 2005. La catástrofe del Prestige. Limpieza y restauración del litoral norte peninsular. Madrid, 288 páginas.

Miranda, F.; Braunschweig, F.; Leitao, P.; Neves, R., Martins, F., and Santos, A., 2000. MOHID 2000, a coastal integrated object oriented model. *Hydraulic Engineering Software VII.* Southampton, UK: WIT Press.

Montero, P.; Blanco, J.; Cabanas, J.M.; Maneiro, J.; Pazos, Y.; Moroño, A.; Balseiro, C.F.; Carracedo, P.; Gomez, B.; Penabad, E.; Pérez-Muñuzuri, V.; Braunschweig, F.; Fernandes, R.; Leitao, P.C., and Neves, R., 2003. Oil spill monitoring and forecasting on the Prestige-Nassau accident. *Environment Canada's 26th Arctic and Marine Oil Spill (AMOP) Technical Seminar.* Ottawa. Canada. pp. 1013–1029.

NOAA, 2002. GNOME. *General NOAA Oil Modeling Environment.* User's manual. Seattle, Washington: Office of Ocean Resources Conservation and Assessment. National Oceanic and Atmospheric Administration.

Peggion, G.; Fox, D., and Barron, C., 2002. A rapidly relocatable prediction system: operational implementation and validation. *In: Proceedings, MTS/IEEE Oceans 2002 Conference,* October 29, 2002, Biloxi, Mississippi, pp. 841–846.

Pingree, R.D. and Le Cann, B., 1990. Structure, strength and seasonality of the slope currents in the Bay of Biscay region. *Journal of the Marine Biological Association of the United Kingdom,* 70(4), 857–885.

Price, J.M.; Reed, M.; Howard, M.K.; Johnson, W.R.; Ji, Z.; Marshall, C.F.; Guinasso, N.L., Jr., and Rainey, G.B., 2006. Preliminary assessment of an oil-spill trajectory model using a satellite-tracked, oil-spill-simulating drifters. *Environmental Modelling & Software,* 21, 258–270.

Reed, M.; Turner, C., and Odulo, A., 1994. The role of wind and emulsification in modelling oil spill and surface drifter trajectories. *Spill Science and Technology Bulletin,* 1(2), 143–157.

Sebastiao, P. and Soares C.G., 2006. Uncertainty in predictions of oil spill trajectories in a coastal zone. *Journal of Marine Systems,* 63, 257–269.

Sobey R.J. and Barker C.H., 1997. Wave-driven transport of surface oil. *Journal of Coastal Research,* 13(2), 490–496.

van Aken, H.M., 2002. Surface currents in the Bay of Biscay as observed with drifters between 1995 and 1999. *Deep-Sea Research I,* 49, 1071–1086.

WAMDIG (WAMDI Group: S.K. Hasselman, P.A.E.M. Janssen, G.J. Komen, L. Bertotti, P. Lionello, A. Guillaume, V.C. Cardone, J.A. Greenwood, M. Reistad, L. Zambresky, and J.A. Ewing), 1988. The WAM model—a third generation ocean wave prediction model. *Journal of Physical Oceanography,* 18, 1775–1810.